3-10-1986

Bathymetric Artifacts in Sea Beam Data: How to Recognize Them and What Causes Them

Christian de Moustier
University of California - San Diego

Martin C. Kleinrock
University of California - San Diego

Recommended Citation

deMoustier, C., and M. C. Kleinrock (1986), Bathymetric artifacts in Sea Beam data: How to recognize them and what causes them, J. Geophys. Res., 91(B3), 3407–3424, doi:10.1029/JB091iB03p03407.

JOURNAL OF GEOPHYSICAL RESEARCH, VOL. 91, NO. B3, PAGES 3407–3424, MARCH 10, 1986

Bathymetric Artifacts in Sea Beam Data: How to Recognize Them and What Causes Them

CHRISTIAN de MOUSTIER AND MARTIN C. KLEINROCK

Scripps Institution of Oceanography, University of California, San Diego, La Jolla

Sea Beam multibeam bathymetric data have greatly advanced understanding of the deep seafloor. However, several types of bathymetric artifacts have been identified in Sea Beam's contoured output. Surveys with many overlapping swaths and digital recording on magnetic tape of Sea Beam's 16 acoustic returns made it possible to evaluate actual system performance. The artifacts are not due to the contouring algorithm used. Rather, they result from errors in echo detection and processing. These errors are due to internal factors such as side lobe interference, bottom-tracking gate malfunctions, or external interference from other sound sources (e.g., 3.5 kHz echo sounders or seismic sound sources). Although many artifacts are obviously spurious and would be disregarded, some (particularly the "omega" effects described in this paper) are more subtle and could mislead the unwary observer. Artifacts observed could be mistaken for volcanic constructs, abyssal hill trends, hydrothermal mounds, slump blocks, or channels and could seriously affect volcanic, tectonic, or sedimentological interpretations. Misinterpretation of these artifacts may result in positioning errors when seafloor bathymetry is used to navigate the ship. Considering these possible geological misinterpretations, a clear understanding of the Sea Beam system's capabilities and limitations is deemed essential.

1. INTRODUCTION

The Sea Beam bathymetric survey system is a multibeam echo sounder developed by the General Instrument Corporation to produce near-real-time high-resolution contoured swath charts of the seafloor down to maximum ocean depth (11 km). Since 1977 when the first system became operational aboard the French R/V *Jean Charcot*, nine other systems have been installed aboard research vessels from the United States, Germany, Japan, and Australia.

Sea Beam systems have proven extremely useful in the study of the geomorphology of the ocean floor and have made possible striking discoveries of features which would not have been detected with conventional single-point depth sounders [e.g., *Macdonald and Fox*, 1983; *Lonsdale*, 1983]. However, after 3 years of experience with the system installed aboard the R/V *Thomas Washington* of the Scripps Institution of Oceanography (SIO), we have discovered a number of artifacts in Sea Beam's contoured output. Their artificial nature has been demonstrated by comparing overlapping Sea Beam swaths and by analyzing digitized raw acoustic data. During four cruises aboard the R/V *Thomas Washington* we used a data acquisition system developed by SIO's Marine Physical Laboratory (MPL) to record digitally the acoustic returns from Sea Beams' 16 preformed beams on magnetic tape. This data set has enabled us to determine the c auses of these artifacts. They do not stem from the vagaries of the contouring algorithm used; rather they are the result of errors in echo detection and processing. In our experience, such detection errors are mostly related to some characteristics of the ocean bottom (e.g., type of substrate or sudden change in slope) or to interference from other sound sources running in parallel with Sea Beam (mostly subbottom profilers: 3.5-kHz echo sounder and seismic sources).

This paper describes several artifacts discovered in Sea Beam data and discusses the associated possible geological misinterpretations. We suggest a number of solutions to improve data quality. We also consider the existence of related artifacts in similar multibeam echo sounders (e.g., the Sonar Array Sounding System (SASS) [*Glenn*, 1970]).

Paper number 5B5427.
0148-0227/86/005B-5427$05.00

2. BACKGROUND: SEA BEAM SYSTEM

Before going into a detailed explanation of the problems found in the SIO system, we briefly review Sea Beam's general framework for the reader unfamiliar with the system. Further discussion of the system are found in the works by *Renard and Allenou* [1979] and *Farr* [1980]. Because a clear understanding of Sea Beam's acoustic geometry and echo processing methods is a prerequisite to analyze its bathymetric output, we have included in the appendices relevant technical information not available in the literature.

As illustrated by the simplified block diagram in Figure 1, the Sea Beam system uses a multibeam narrow beam echo sounder and an echo processor (EP) to generate in near-real time, contour maps of the ocean floor. A 20-element projector array mounted along the ship's keel sends out a 7-ms pulse of 12.158 kHz at intervals that are integral multiples of 1 s. The transmission period is usually determined by an analog graphic recorder. The receiving unit lies athwartships and consists of 40 line-hydrophone arrays whose long axes are oriented fore-aft. The resulting transmit/receive geometry is illustrated in Figure 2. In Figure 2, vertical cross sections of theoretical

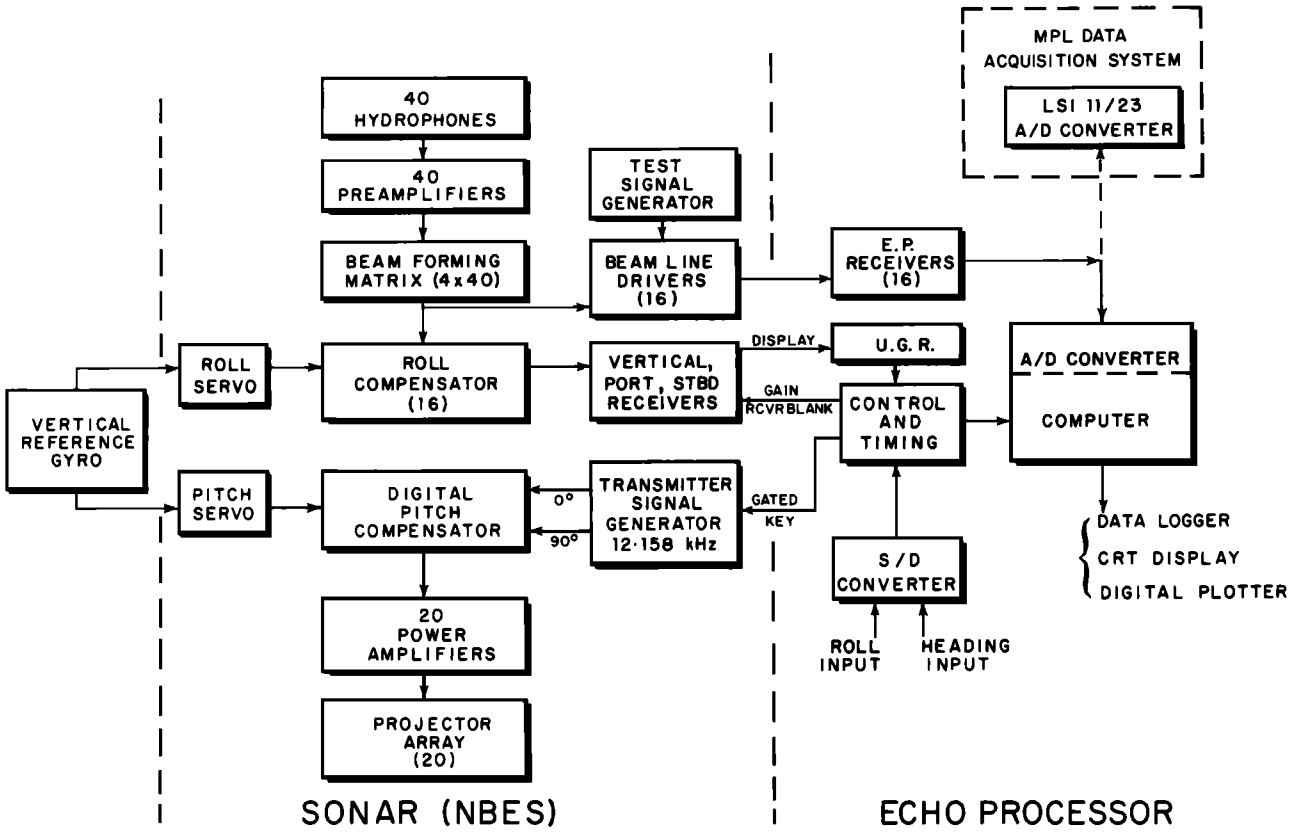

Fig. 1. Block diagram of the Sea Beam system showing the narrow beam echo sounder and the echo processor. The position of the MPL data acquisition system is shown for reference.

beam patterns are shown for both the projector (Figure 2*a*) and the receiver (Figure 2*b*) arrays. The transmit beam pattern spans 54° athwartships by 2 2/3° in the fore-aft direction. It is pitch stabilized within a range of ±10° of pitch. There is no pitch compensation for the receive beam pattern, instead it spans 20° in the fore-aft direction to accommodate pitch angles of ±10°. The athwartships beam width is 2 2/3°. Sea Beam receives with 16 fixed preformed beams obtained by electronically steering this 20° x 2 2/3° beam at athwartships intervals of 2 2/3° between ±20° of incidence. In this configuration there is no beam along the ship's vertical axis; rather two of the beams point at 1 1/3° on either side of this axis.

The acoustic energy received at the ship comes from the intersection of the transmit and receive beam patterns. This appears in Figure 2*c* as 16 squares 2 2/3° on a side. Figure 2*c* is only meant to illustrate the angular relationship between the main lobe of the transmitted beam pattern and the main lobes of the 16 preformed beams. Actual footprints are not rectangles or squares; they are ellipses whose areas increase away from vertical incidence. Since depths are ideally determined at the center of each of the preformed beams, the maximum swath width corresponds to 73% of the water depth.

The beam-forming operation described above generates 16 acoustic signals. These are sent to the EP receivers where they are filtered, rectified, amplified, and transferred to the Sea Beam computer (Figure 1). Figure 3 shows a typical output of the 16 EP receivers. Each waveform corresponds to a preformed beam and is accordingly numbered from the center out (1-8) on port and starboard. In Figure 3 the ridge of synchronous returns (see arrow labeled "side lobe") corresponds to energy from the near-specular direction (tallest return) entering the side lobes of the other beams. The 16 bottom return signals form a parabola, indicating a flat portion of seafloor. These data have been digitized and recorded on magnetic tape with a separate data acquisition system (Figure 1) built around an LSI 11/23 minicomputer, in an experiment conducted by MPL to measure acoustic backscatter from the deep seafloor. They have proven invaluable to evaluate the performance of the EP because Sea Beam only retains depths and cross-track horizontal distances.

In the Sea Beam computer, 16 such waveforms are simultaneously digitized at a frequency of 300 Hz per waveform. This corresponds to one digitization cycle every 3.33 ms or 2.5 m of slant range assuming a sound velocity of 1500 m/s. Consequently, slant range and therefore depth determination resolution is limited to 2.5 m. While it digitizes the acoustic data, the computer also performs several echo processing tasks. For each digitization cycle these tasks are receiver gain correction, refraction correction, roll compensation, detection threshold level computation, and echo detection. Automatic bottom-tracking gates (one for each beam) determine a time window during which a return is expected on any one beam based on previous sounding history. A return is detected if it falls within the gates and lies above the threshold.

In general, the threshold level is computed to ride

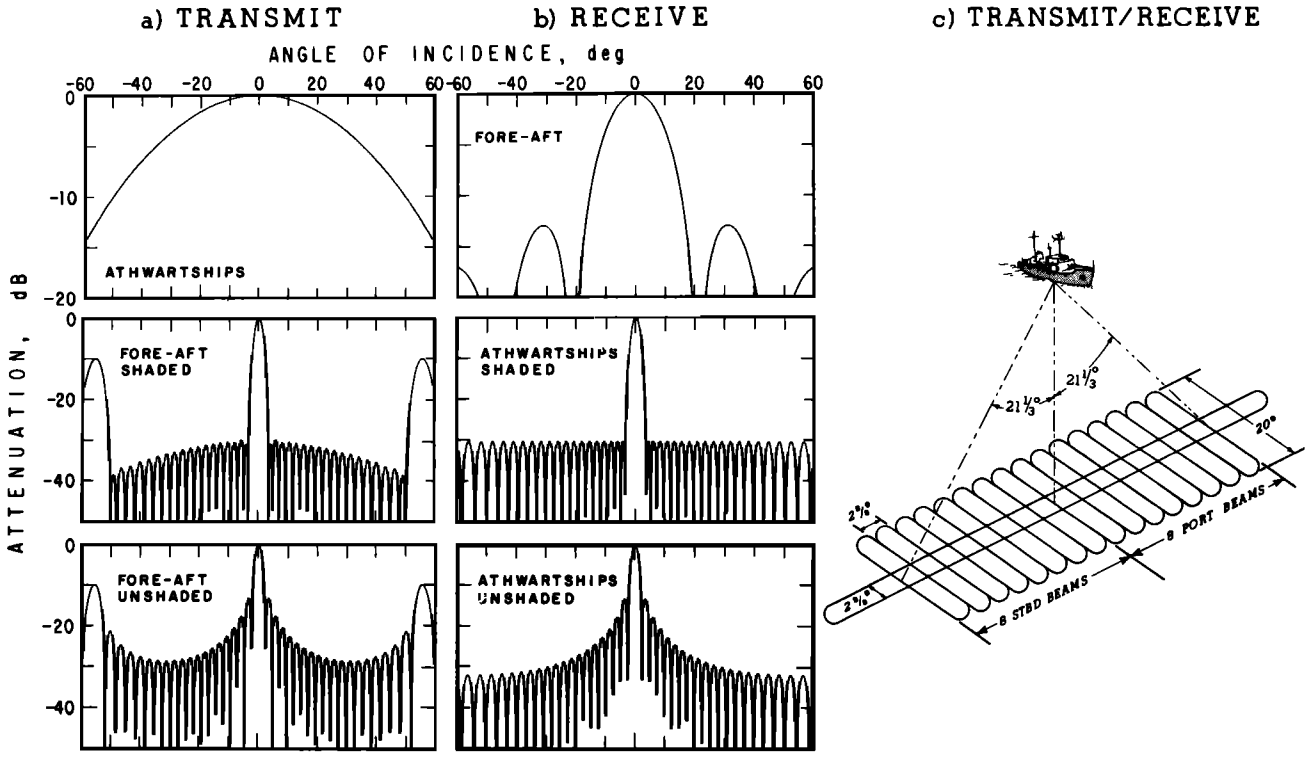

Fig. 2. Sea Beam transmit/receive geometry. Computed beam pattern cross sections in the athwartships vertical plane centered on the array and in the vertical plane passing through the ship's fore-aft axis are shown for (*a*) the projector array and (*b*) the receiver array. The effect of Dolph-Chebyshev amplitude shading is also illustrated. (*c*) A summary cartoon showing the angular relationship between the main lobe of the transmitted beam pattern and those of the 16 preformed beams.

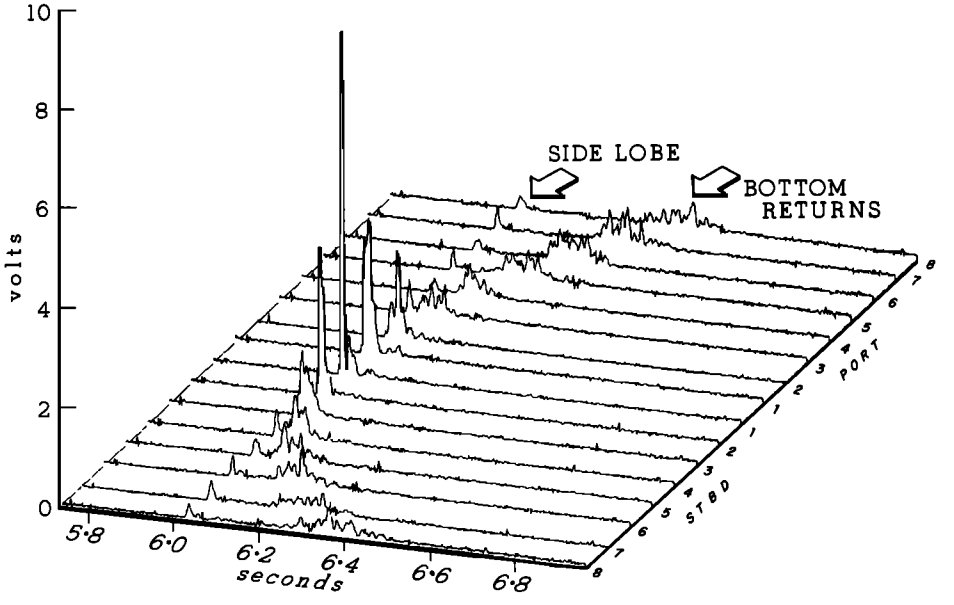

Fig. 3. Acoustic signal envelopes of the 16 preformed beams at the output of the Sea Beam echo processor receivers. The time axis represents seconds after transmission. The vertical axis in volts represents the voltage equivalent of the sound pressure level at the receiver array, corrected for acoustic transmission losses in the water column by a time-varied gain (TVG). No roll compensation, recording gain, or receiver gain corrections have been applied to the data at this stage. Such data are recorded digitally on magnetic tape every transmission cycle, along with time, TVG, and ship's roll.

above the noise, above the side lobe response to a strong specular return, and above potential noise bursts interfering with bottom echo detection. A manual threshold can also be entered by the Sea Beam operator. As we shall see in the following sections, thresholding and gating are two critical operations in the echo processing. A more detailed description of Sea Beam's echo processing may be found in Appendix B.

For each roll-compensated beam having sufficient signal to noise ratio, a slant range R is calculated by computing the center of mass of all the detected signal samples for that beam and by multiplying the corresponding arrival time by 750 m/s. Knowing the slant range R and the stabilized beam angle Ψ, a simple calculation yields the depth Z and the cross-track horizontal distance Y:

$$Z = R \cos \Psi \qquad Y = \frac{C_a}{C_n} R \sin \Psi$$

where C_a is the mean sound velocity obtained by averaging the values of the sound velocity profile from the surface to the average bottom depth (in uncorrected meters) and C_n is the nominal sound velocity in water (1500 m/s). The depth Z is given in uncorrected meters referenced to a sound velocity of 1500 m/s. The cross-track horizontal distance Y is a true distance because it is corrected for both refraction and travel time.

Finally, the (Z,Y) coordinates for each validated beam are output as a cross-track bottom profile on the EP cathode ray tube (CRT) display. The depths are also used to update the bottom-tracking gates on each beam for the next transmission cycle.

The depths and cross-track horizontal distances for each transmission cycle are logged on a magnetic storage medium (disk or tape) along with time and ship's heading, as well as output in near-real time (~1 min delay) on paper as a contour chart by an 11 inches digital swath plotter. In the following, we will refer to the (Z,Y) data as the raw Sea Beam data.

The Sea Beam echo-processing sequence outlined here will vary depending on the EP mode chosen by the operator. Three modes are available. Mode 1 is essentially a start-up mode during which no data logging or contour plotting are performed. The EP displays the vertical beam depth and the CRT shows unprocessed echoes on the 16 preformed beams. The detection threshold used in mode 1 is the highest of the noise threshold, the side lobe threshold, or the threshold entered by the operator. Mode 2 is a semiautomatic EP operation with data logging and contour plotting. The CRT displays processed data in the form of a cross-track bottom depth profile, but the operator controls the tracking gates' width and center. Mode 3 is a completely automatic version of mode 2. It is the mode in which the EP usually operates during bathymetric survey work. A very important and poorly documented difference exists between the detection threshold level determination of mode 1 and that of modes 2 and 3. In modes 2 and 3, a nonzero threshold level input by the operator supercedes any other threshold computation. It is therefore imperative that the manual threshold be set to zero when in mode 2 or 3. Failure to do so results in the EP tracking the side lobe response any time a specular return is present on one of the 16 preformed beams or, if the manual threshold is set high enough, in loss of data.

On most ships equipped with Sea Beam the bathymetry data are merged with ship navigation (transit satellite navigation and dead reckoning, or NAVSTAR Global Positioning System navigation when available) by another computer aboard the ship and recontoured along the ship's track on a 30 inches digital plotter with a delay time of about 2 min. This gives the surveyor the ability to effectively control ship navigation and track spacing by looking at the contours plotted. A second stage of data postprocessing, done on ship or ashore, consists of adjusting the navigation to fit corresponding contour lines on adjacent tracks and of regridding the entire data set to produce a map. When navigation comes from the Global Positioning System there is virtually no need for adjustments. These operations usually smooth the raw Sea Beam soundings by averaging along track over a certain number of transmission cycles (often five) to produce more even grid spacing along versus across the ship's track, thus removing most of the jitter apparent on near-real-time swath plots. However, when system errors cause bad soundings, the resulting fictitious bathymetry will often not average out as we shall show in the following sections. Therefore in order to assess the validity of suspicious Sea Beam bathymetry, an investigator needs to refer to the raw data and use any corroborating information available. When only the raw data are available, as is often the case, such assessment requires a clear understanding of the processing performed by the Sea Beam computer on the digitized acoustic signals.

3. SEA BEAM BATHYMETRIC ARTIFACTS: EXAMPLES, EXPLANATIONS, AND GEOLOGICAL IMPLICATIONS

Sea Beam has been used extensively in the past several years to study the morphology, tectonics, volcanology, and sedimentology of the seafloor. So many Sea Beam surveys have been run that a complete list is too large for inclusion here; therefore we only reference some of the more recent works. Bathymetric charts produced from Sea Beam data have been used as base maps for more detailed studies using deeply towed instrument packages such as MPL's Deep-Tow [*Spiess and Lonsdale*, 1982; *Spiess et al.*, 1984; *Hey et al.*, this issue] and manned submersibles such as Woods Hole Oceanographic Institute's (WHOI's) DSRV *Alvin* and DSRV *Cyana* of the Institut Français de Recherche pour l'Exploitation de la Mer (*IFREMER*) (formerly Centre National pour l'Exploitation des Océans (*CNEXO*)) [e.g., *Ballard and Francheteau*, 1983; *Francheteau and Ballard*, 1983]. Many surveys covering fairly large areas (hundreds of square kilometers) with nearly total coverage have lead to valuable insights into the processes at spreading centers [e.g., *Hey et al.*, this issue; *Crane et al.*, 1985; *Macdonald et al.*, 1984; *Mammerickx*, 1984; *Lonsdale*, 1983], transform faults [e.g., *Gallo et al.*, 1984; *Detrick et al.*, 1984] trenches [e.g., *Shipley and Moore*, 1985; *Lewis et al.*, 1984], microplates [e.g., *Hey et al* 1985, *Naar and Hey*, this issue], seamounts [e.g., *Fornari et al.*, 1984], and submarine canyon systems [e.g., *Lewis et al.*, 1984]. Sea Beam's regional depiction of the seafloor in these areas has been extremely useful.

In most cases, the finer-scale Sea Beam bathymetry is

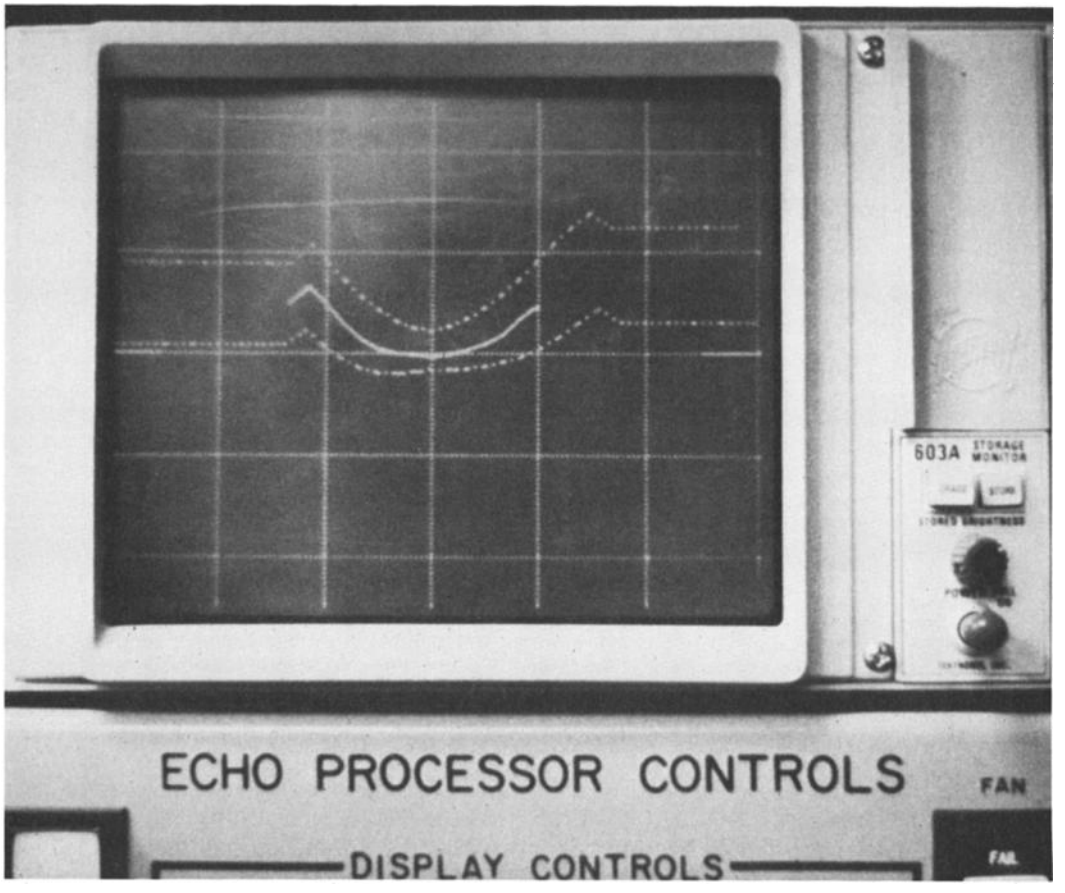

Fig. 4. Echo processor CRT display showing a cross-track bottom profile (solid trace) characteristic of a "tunnel" effect. The dashed traces represent the upper and lower positions of the automatic bottom-tracking gates. The vertical scale is 200 m per division. The horizontal scale is compressed to accommodate a reception beam width spanning 80° (40° actual beam width with ±20° for roll).

dependable and is reproducible on overlapping swaths. However, given the existence of the bathymetric artifacts discussed in this paper, investigators should be cautious when studying bathymetric details on the scale of hundreds to thousands of meters. This is particularly important for surveys of large areas where bathymetric and structural data are interpolated between widely separated Sea Beam swaths. Misinterpreting any of these artifacts as true bathymetric features could also result in positioning errors when the vessel is navigated by comparison of real-time bathymetry with compiled charts.

In the following we discuss three types of bathymetric artifacts resulting from echo-processing errors. These errors are due to internal factors such as side lobe interference or malfunction of the bottom-tracking gates or to external interference from other sound sources. In each case we present evidence of artifacts through Sea Beam data samples, explain their cause, and indicate their geological implications.

3.1. *Side Lobe Interference*

Renard and Allenou [1979] recognized side lobe interference as a potential problem in Sea Beam (e.g., Figure 21 in their paper). The interference is characterized by small apparent slope fluctuations on seafloor dipping perpendicular to the ship's track, and it typically affects only a few beams. A more serious problem occurs when the seafloor surveyed is relatively flat and Sea Beam renders it as a trough (the "tunnel" effect [*Smith*, 1983]). This is seen as a concave-up arc on the cross-track CRT bottom profile in Figure 4. To understand this artifact, consider the Sea Beam acoustic data shown in Figure 5 which is identical in format to Figure 3. Note that the side lobe level is much higher in Figure 5 than in Figure 3. If the EP is in mode 3 and a nonzero manual threshold level has been entered by the Sea Beam operator, the system does not calculate a noise or a side lobe threshold. It therefore tracks the side lobe response when present and when above the manual threshold level. Arrival times are then synchronous on all beams as if coming from a concave-up horizontal half cylinder. Figure 6 shows an example of the resulting bathymetry.

The apparent relief of the "tunnel" walls in this example ranges from 40 m to 100 m, although theoretically it may be as much as 6% of the water depth. The actual seafloor morphology in this area is not precisely known because the MPL acoustic data acquisition system was not available during this survey. This area is believed to be generally flat with indications of roughly north-south abyssal hill

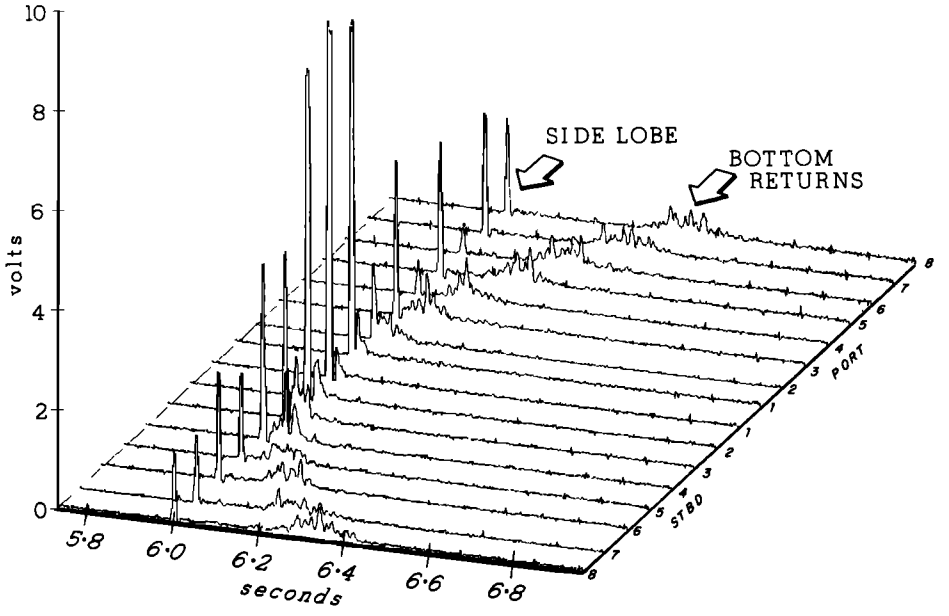

Fig. 5. Acoustic signal envelopes of the 16 preformed beams at the output of the Sea Beam EP receivers. The format is identical to that of Figure 3. The ridge of synchronous returns due to side lobe response is much more pronounced in this figure than in Figure 3 because it is due to a stronger near-specular return (starboard beam 1, which is clipped in this figure)

trends. Such "tunnels" might be mistaken for troughs between abyssal hills or submarine channels, but investigators would recognize them as artificial because the trough axes follow the ship track, independent of course changes.

The "tunnel" effect can also occur when a zero manual threshold has been entered, even though the system computes a noise and a side lobe threshold. In the example given in Figure 5, we identify two processes which combine to defeat the side lobe rejection scheme outlined in the appendices. First, a very strong specular return was received at the hydrophones, indicating a highly reflective seafloor. Second, the EP receiver outputs were found to saturate at 8.5 V rather than the specified maximum output of 10 V [*de Moustier*, 1985*a*]. As a result the peak amplitude on the specular return is clipped (starboard beam 1 in Figure 5). The side lobe threshold level computed on a clipped peak only partially removes the side lobe response, and the remaining portions of side lobe response bias the center of mass calculation in their direction given the comparatively low signal to noise ratio of the real backscattered bottom returns. Eventually, the

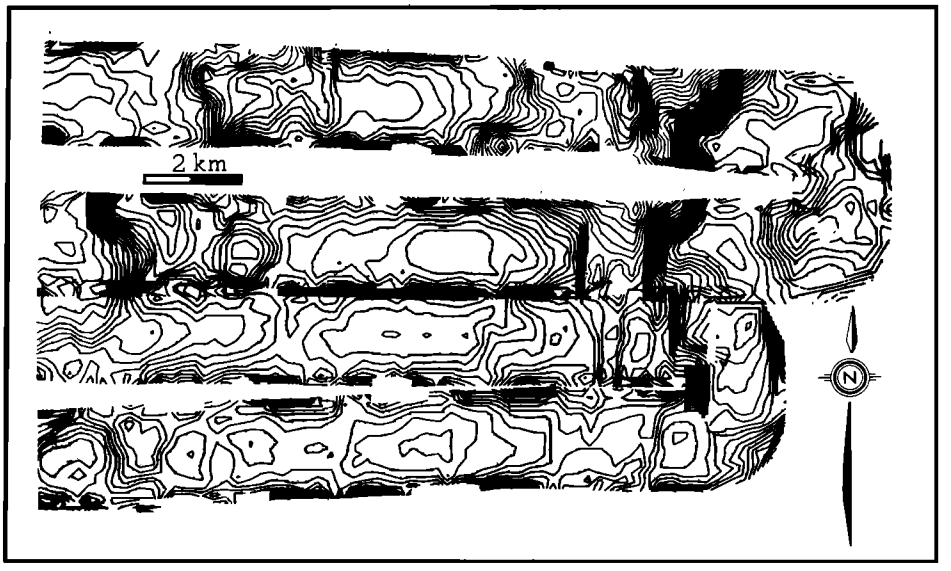

Fig. 6. The "tunnel" effect. Four portions of Sea Beam swaths adjusted for navigation are shown here to illustrate the effects of a non-zero manual threshold when the echo processor runs in mode 2 or 3. Sea Beam's rendition of the bathymetry is seen as a trough approximately centered on the ship's track. This trough persists through changes in the ship's course, thereby indicating its artificial nature. Fictitious gullies also appear on slopes updip as well as downdip (best seen in the upper right section of this figure). Contour interval is 10 m, and tick marks point downhill.

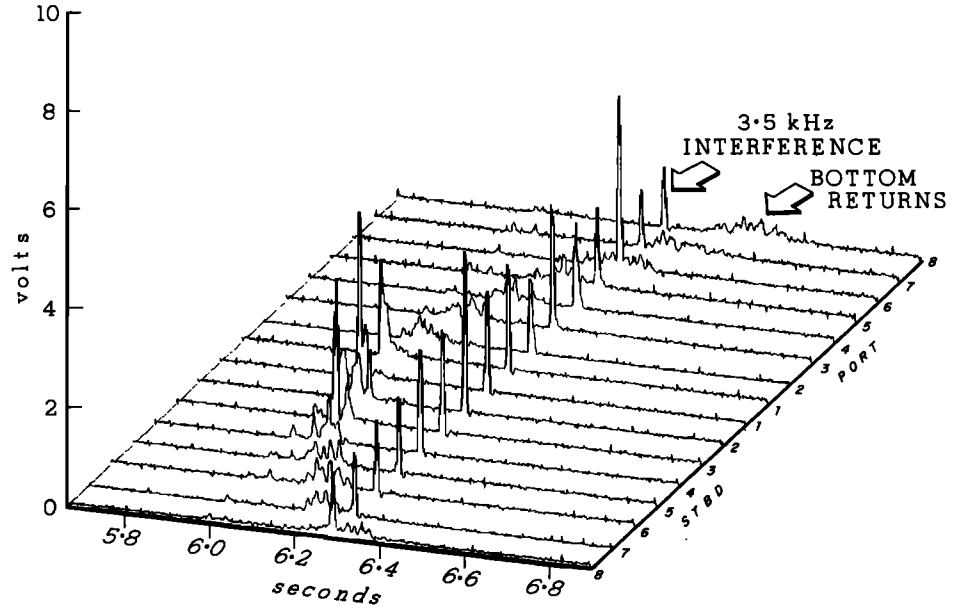

Fig. 7. Evidence of a 3.5-kHz echo sounder transmitting during a Sea Beam reception cycle. The corresponding noise burst appears as a synchronous ridge across all 16 preformed beams. The format is the same as that of Figure 3. A noise burst ridge differs from a side lobe response ridge in that the levels of the peaks are more or less constant for the former, while a marked difference in level exists between the specular return and its corresponding side lobe response (Figures 3 and 5). The differences in level seen in this figure are due to differences in receiver gains which were not corrected.

system tracks the side lobe response instead of the bottom, creating a troughlike feature. The limiting case is that of a mirrorlike hard surface from which there is no backscatter. In this case, one would see only a strong specular return and a synchronous ridge of side lobe returns. However, most of the time the bottom offers some roughness on the scale of Sea Beam's 12-cm acoustic wavelength, and the signal to noise ratio of the backscattered returns is sufficient to track the bottom correctly.

It is important to note that the prerequisite for side lobe interference is a strong near-specular return on any one of the preformed beams. The bottom does not necessarily have to be flat (e.g., *Renard and Allenou's* [1979] example). In cases where the side lobe response is well separated from the bottom return (e.g., port beam 8 in Figure 5), it usually falls outside the tracking gates. When the side lobe and the actual bottom returns are close together or overlapping, as is usually the case on returns adjacent to the near-specular return (e.g., port beam 1 in Figure 5), the system has no way of differentiating between side lobe response and bottom return. Rejecting the side lobe response will most likely cancel some of the bottom return, resulting in a slightly erroneous depth determination. Likewise the computed depth is in error if the side lobe response is not rejected. The errors are small (~5 m) for beams oriented in the near-specular directions, and increase away from specular incidence due to the lengthening of the backscattered return signal duration (pulse stretching) with both beam angle and depth.

3.2. *Interference From External Sound Sources*

External sound sources interfere with the Sea Beam system when they transmit while Sea Beam is receiving echoes from the seafloor. Figure 7 shows an example of a 3.5-kHz echo sounder interference as seen in the acoustic data. It appears as a synchronous ridge across the 16 preformed beams. This is a classical example of a noise burst. As for the side lobe interference, the dynamic thresholding used to reject such noise bursts has side effects which produce fictitious bathymetry, examples of which can be seen in Figure 8. The portion of the noise burst which is well separated from the actual bottom returns are effectively rejected by dynamic thresholding or by gating. However, where signal and noise burst overlap, canceling the noise burst also cancels part of the signal and skews the center of mass calculation for that return. As the noise burst slowly progresses through the reception cycle over a number of pings, bathymetric peaks appear on the contoured output in the direction of the beams which point away from specular incidence. The near-specular directions are not affected as much since pulse stretching is minimal, thereby reducing the margin for error.

The bathymetric peaks are typically short wavelength (hundreds of meters) and may vary in amplitude from tens to hundreds of meters. The more pronounced of these peaks are often clearly spurious and extremely steep and sharp; such features are geologically unlikely, and investigators will readily disregard them. Smaller-amplitude artifacts are less obvious and might be mistaken for small volcanic cones or large hydrothermal mounds. One common, although not ubiquitous, characteristic of these artifacts is the simultaneous occurrence of more than one in different parts of the swath. Investigators aware of the potential for these phenomena are unlikely to misinterpret them. Seismic sound sources such as water guns produce similar effects, but no observable interferences have been reported with air guns, probably because they do not output enough acoustic energy in the 12-kHz frequency band [*Smith*, 1983].

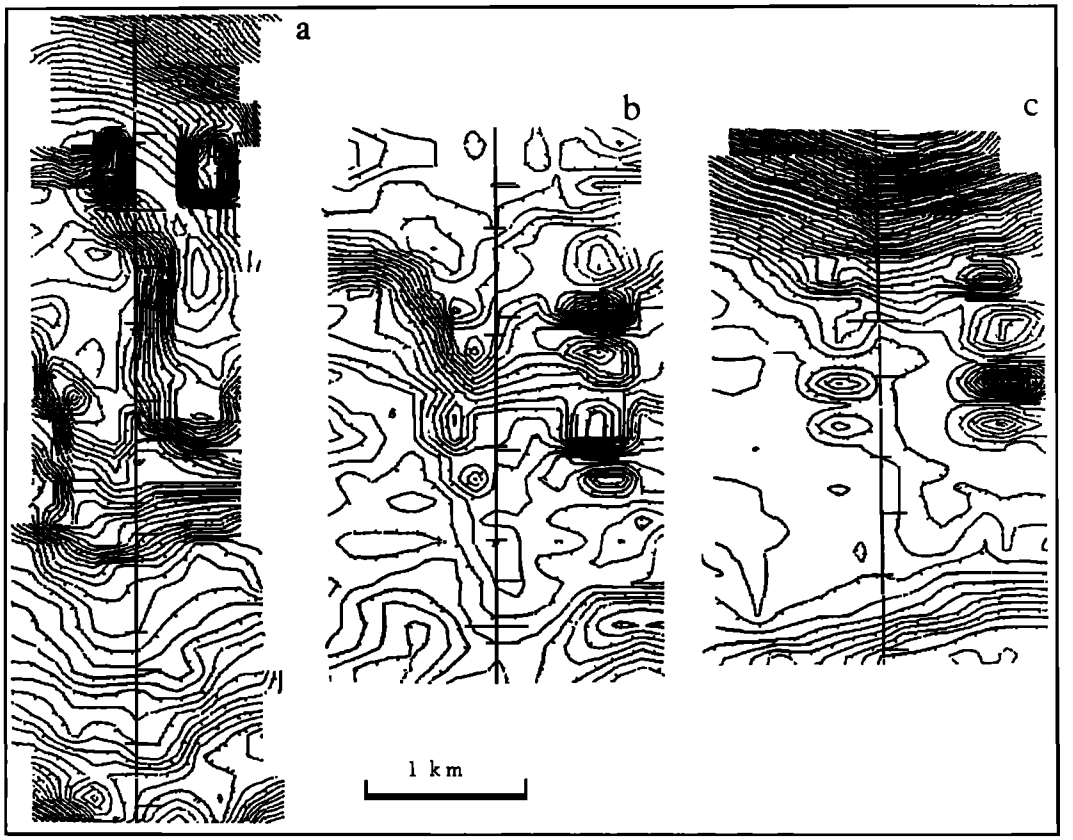

Fig. 8. Examples of contoured swath plots showing the results of external sound source interference. Artifacts can be recognized as individual peaks on one or both sides of the ship's track (center line in all three plots). Contour interval is 10 m, and tick marks point downhill.

A special case of interference from external sound sources exists for 12-kHz bottom transponders. Figure 9 shows an example of such interference with evidence of a transponder trace on the corresponding analog center beam depth profile. The flat sedimentary bottom over which this data was taken illustrates the progression of the interference. The interference enters the outer beams' tracking gates while falling outside those of the near-specular beams. This is evidenced in Figure 9*a* by a central ridge followed by two small mounds on either side of the ship's track. The small mounds would be difficult to identify as artificial, were it not for evidence from the analog record (Figure 9*b*) which shows the transponder trace intersecting the center beam depth profile at the corresponding time. Due to their small size, these artifacts would probably not be considered very significant, although some might mistake them for satellite cones or hydrothermal mounds.

The situation of this example is uncommon because the ship was maneuvering at about 1.5 knots over a bottom transponder network while towing the Deep-Tow instrument package. However, it may become more common with the Sea Beam system installed on WHOI's R/V *Atlantis II*, the mother ship for the manned DSRV *Alvin* which is often navigated using 12-kHz transponders. At normal survey speeds (~10 knots) this artifact would be greatly reduced. Similar artifacts due to interference from the direct or the bottom bounced signal of a 12-kHz pinger have also been noted during dredging or coring operations.

3.3 "*Omega*" *Effects and Data Gaps*

Most Sea Beam users are aware of the possibility of side lobe or external sound source interference in the system. A lesser known and more insidious artifact has been found to occur on sloping bottoms producing contours resembling the capital Greek letter omega (Ω) [*Kleinrock et al.*, 1984] or data gaps. They are generally characterized by an arcuate plateau followed by a steep, curvilinear scarp. They occur within a single Sea Beam swath, commonly near the center, and have lateral dimensions of hundreds to thousands of meters. The plateaus may be peaked (Plate 1*e*) or flat (Plate 1*d*). (Plate 1 is shown here in black and white. The color version can be found in the separate color section in this issue.) The scarp may be semicircular (Plate 1*d* the classic Ω shape) or irregular (Plate 1*f*). "Omegas" sometimes evolve into or are associated with data gaps (Plate 1*b* and 1*g*) and can be created on sides of seamounts (Plate 1*c*) as well as relatively straight scarps.

Plate 1*a* shows the problem clearly. In this case, the same portion of seafloor has been surveyed in three different directions. The arrows indicate the direction of ship travel. In Plate 1*a*, sections 1 and 2, Sea Beam's rendition of the bathymetry is nearly identical for opposite ship courses in the along slope direction. The bathymetry

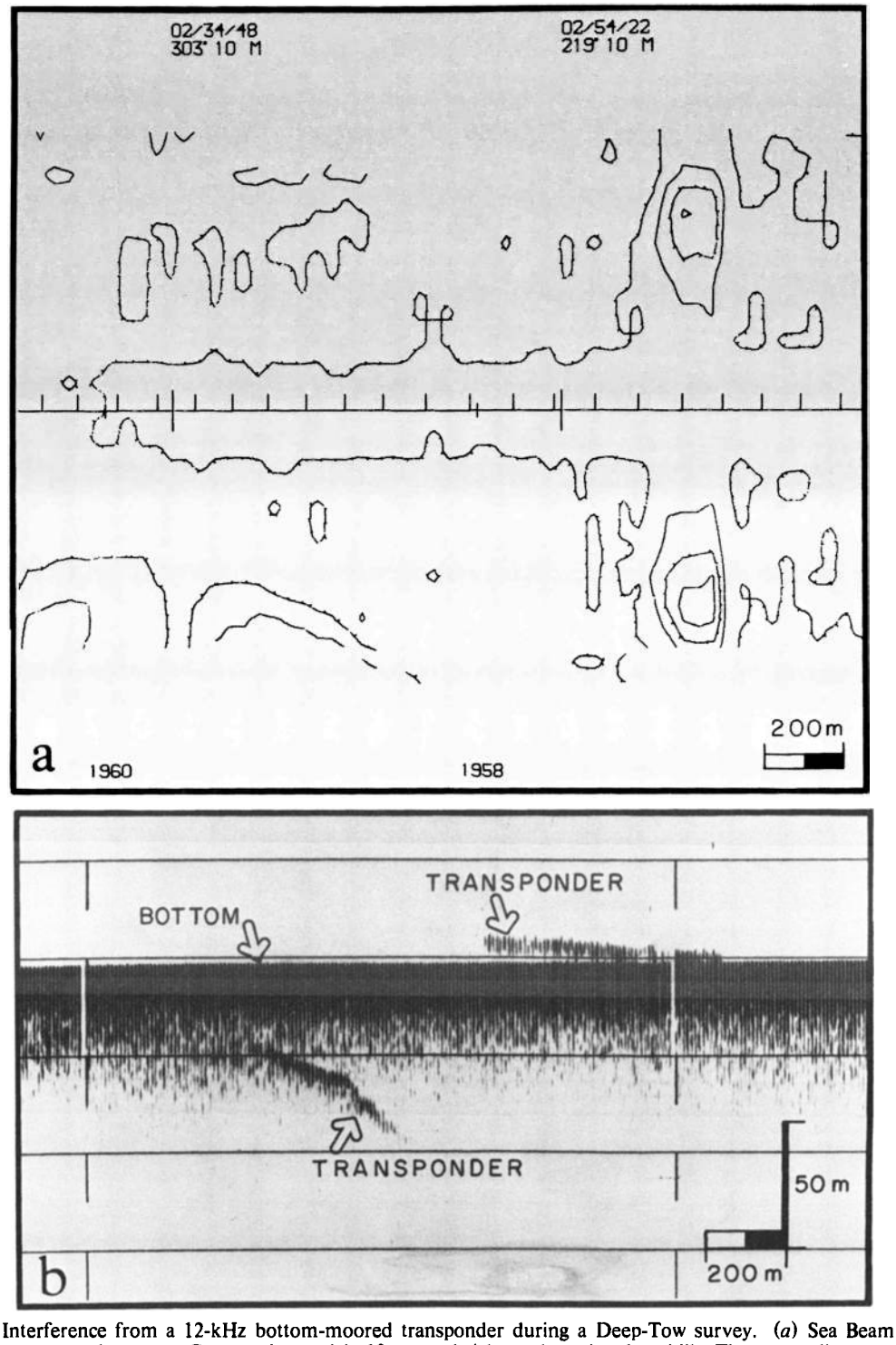

Fig. 9. Interference from a 12-kHz bottom-moored transponder during a Deep-Tow survey. (*a*) Sea Beam near-real-time contoured output. Contour interval is 10 m, and tick marks point downhill. The center line represents the ship's track. On this line, short ticks above the ship's track are spaced 2 min apart, long ticks refer to information at the top of the plot (time [hour/min/s], ship's heading, contour interval in meters), and short ticks centered on the track refer to center beam depth in meters indicated at the bottom. (*b*) Analog graphic recorder output displaying Sea Beam's center beam depth profile and the trace of the 12-kHz transponder. The horizontal scale is matched in time to that of Figure 9*a*. The artifact can be seen in Figure 9*a* as the two small mounds on either side of the ship's track.

is markedly different when the ship track runs downdip (across a slope in the down hill direction) (Plate 1*a*, section 3). In all the colored contour plots shown, contour lines have been smoothed by averaging over five transmission cycles. While inspecting the raw Sea Beam data, we noticed unrealistic variations in depth from one ping to the next as well as missing soundings in the data of Plate 1*a*, section 3. No evidence of external interference was

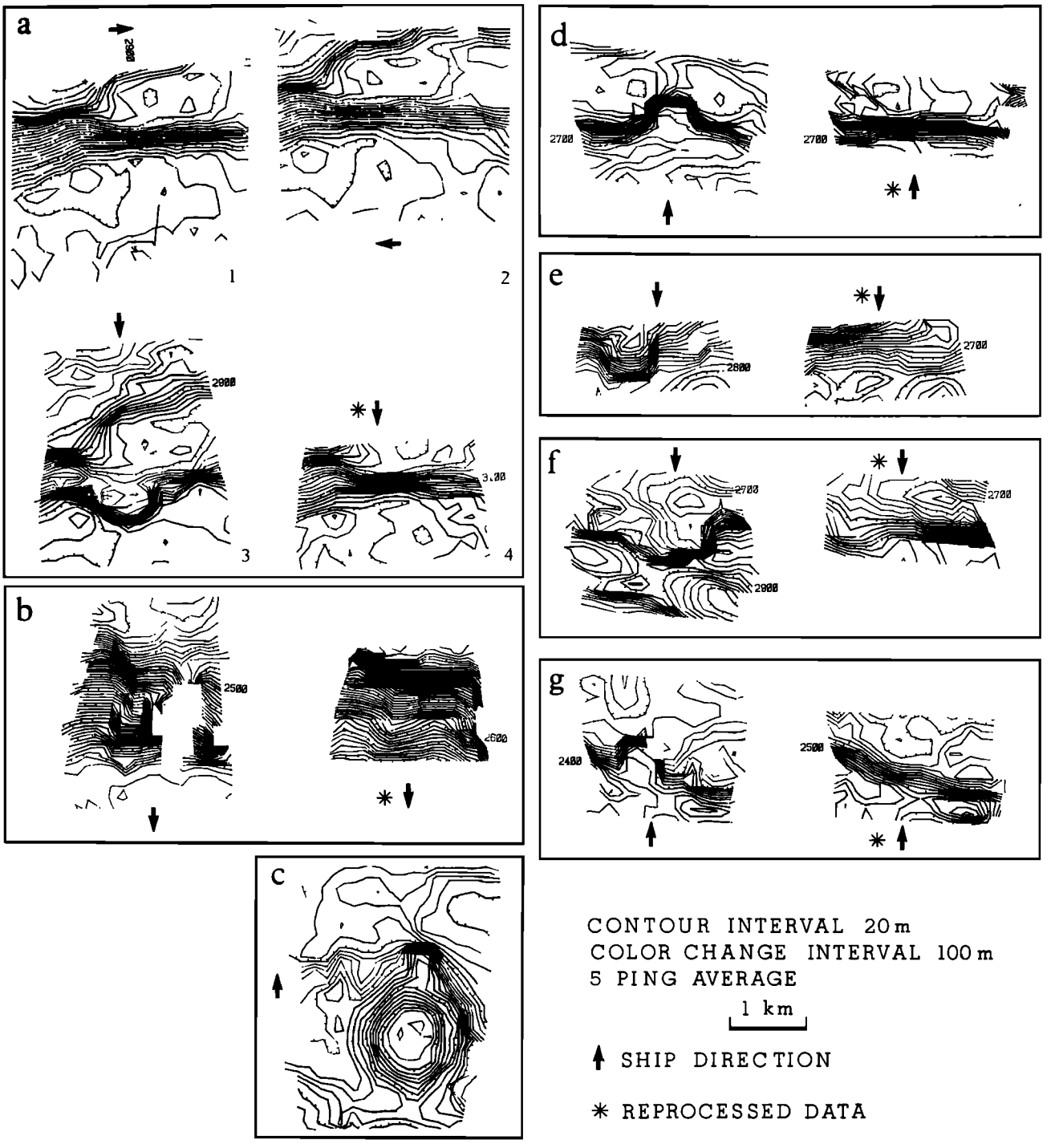

Plate 1. "Omegas" and gaps. (The color version and a complete description of this figure can be found in the separate color section in this issue.)

found in the acoustic data. After computing depths and cross-track distances from this acoustic data, we contoured them using the same postprocessing software used throughout Plate 1. The resulting bathymetry shown in Plate 1*a*, section 4 matches that seen in Plate 1*a*, sections 1 and 2. Sea Beam was clearly in error when the ship track ran downdip.

A combination of three factors may be responsible for this artifact. First of all, the automatic bottom-tracking gates do not open fast enough upon a sudden change of bottom slope. As a result, data are lost for points falling outside the gates. Second, when going downdip across a slope the fore-aft transmit beam pattern geometry (Figure 2*a*) is such that acoustic energy from the side lobes may ensonify the slope in the specular direction. Although this transmitted energy is about 25 dB lower than that transmitted in the main lobe in the true vertical direction, it becomes significant due to the angular dependence of

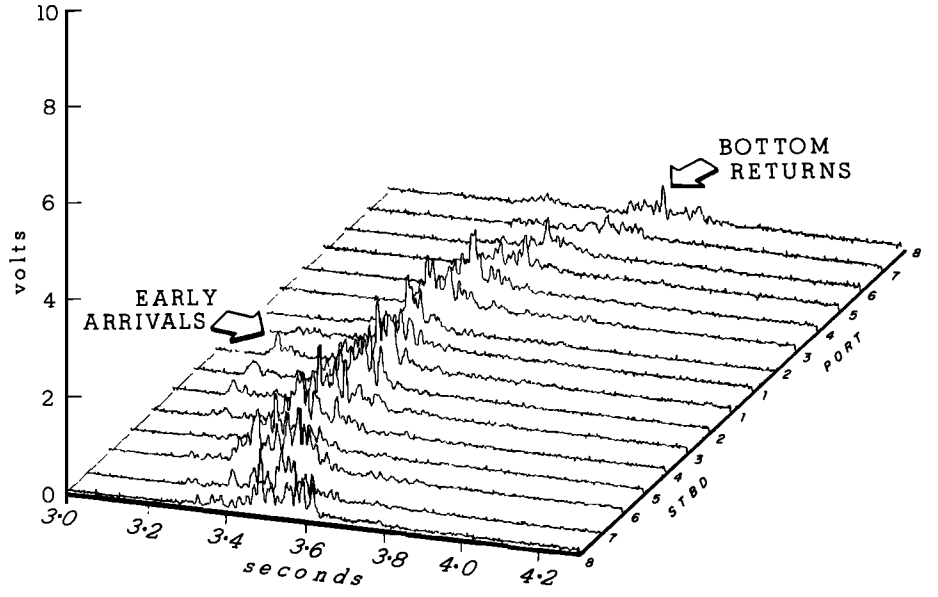

Fig. 10. Evidence of transmit beam pattern side lobe interference in the digitized acoustic data. Early arrivals corresponding to near-specular returns from transmitted side lobe energy are best seen on starboard beams 1-3. These data correspond to the "omega" effect shown in Plate 1*e*. The format is the same as that of Figure 3.

backscattering. Measurements have shown that one can expect a drop of 10-15 dB in the acoustic backscatter between normal (specular) incidence and 20° incidence [*Patterson* 1969; *Urick*, 1983]. For a flat bottom the acoustic backscatter due to side lobe transmitted energy is negligible compared to the returns due to the main beam in the specular direction. This is no longer true when the bottom slope is such that the side lobes of the transmit beam pattern point in the specular direction as in this case. Because the receiving beam pattern is 20° wide in the fore-aft direction (Figure 2*b*), early returns are received as seen in Figure 10. Given the proper threshold and sufficiently narrow tracking gates (which is the case when the bottom has remained relatively flat for some time), the system tends to track these early returns, creating a plateaulike feature. At some point the signal to noise ratio

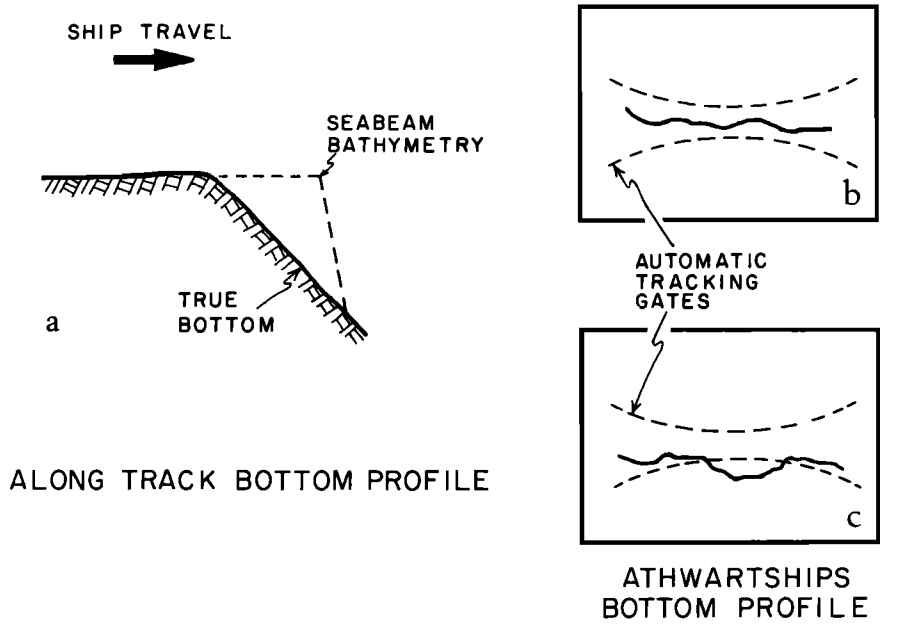

Fig. 11. Cartoons of bottom profiles associated with "omegas" and gaps. (*a*) Along-track bottom profile of an "omega" artifact. Sea Beam's rendition of the bathymetry, shown by the dashed line, is a plateau followed by a steep scarp. (*b*), (*c*) Bottom-tracking gates conditions as would be seen on the echo processor's CRT. In Figure 11*b* the athwartships bottom profile (solid line) lies inside the tracking gates (dashed lines). This is the normal mode of operation when the echo Processor is in mode 3. It is also what one would see were an "omega" effect present. In Figure 11*c* the athwartships bottom profile lies partially outside the tracking gates, and the corresponding data points are lost. This situation is characteristic of data gaps.

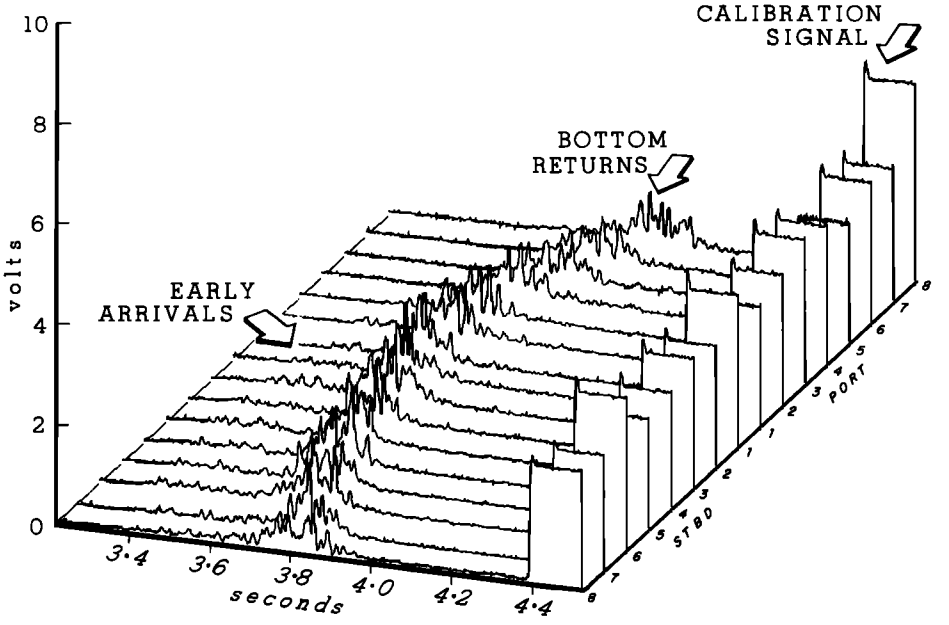

Fig. 12. Receivers' gain calibration. The raised signals seen at the end of each of the 16 preformed beam returns represent calibration signals injected into each receiver to determine its gain setting. Here one can appreciate the usefulness of the echo processor gain correction which brings all receivers to a common gain level. The format of this figure is identical to that of Figure 3.

of these returns becomes too low, and the system fails to detect an echo until the tracking gates open wide enough to recover the real bottom. Hence a sharp drop in depth results at the end of the plateau as shown in the cartoon of Figure 11*a*.

Consider two possible tracking gate conditions: a normal condition where the instantaneous bottom profile is contained within the gates (Figure 11*b*) and a condition where part of the profile falls outside the gates (Figure 11*c*). The latter produces a data gap as seen in Plates 1*b* and 1*g* where the onset of an "omega" effect immediately precedes the gap. Apparently, the dip of the bottom increased too rapidly for the "omega" effect to develop fully, and a gap appeared because the gates simply could not open fast enough. Such gaps exist in Sea Beam data on updip as well as downdip ship tracks; however, in our data we have seen "omega" effects only for downdip ship tracks. This was confirmed at sea when an observed "omega" effect on a downdip track was immediately resurveyed updip, and no "omega" was detected. The most likely explanation for this asymmetry comes from the fact that the gates are always lagging upon a sudden change in bottom slope. Downdip, the gates track from the left in Figure 10, and they are therefore likely to track early returns. Updip, the gates track from the right in Figure 10 so they have a better chance to track bottom returns instead of early arrivals. Also the gates have more time to adjust at the base of rising slopes due to the accumulation of talus. We cannot specify a slope range for which an "omega" effect occurs because this effect varies with ship's speed and depends on the side lobe level on the transmit beam pattern of the Sea Beam system considered. As ship speed is reduced, the tracking gates have more transmission cycles to adjust to a sudden drop in slope, and the "omega" effect is less likely. Our data shows "omega" effects on slopes between 30° and 45° for ship speeds of about 10 knots, but similar though subtler artifacts seem to appear on gentler slopes, perhaps as low as 15°.

The tracking gates and the transmit/receive acoustic geometry are the two main factors contributing to the "omega" effect. A third factor is related to the half-hour calibration of the EP receivers. In several instances, we found that this calibration occurred immediately prior to an "omega" effect. Figure 12 shows the onset of a receiver gain calibration sequence just at the end of a reception cycle. The following transmission cycle showed only the calibration signals. Inspection of the raw Sea Beam data showed that no data had been logged for these two cycles even though one would have expected the first (Figure 12) to have been processed by the EP. As a consequence, data are lost for two transmission cycles every half hour. Moreover the tracking gates are not updated during this time. A coincidental increase in bottom slope puts the EP in a difficult bottom-tracking situation which, given the appropriate slope angle, ship direction, and signal to noise ratio in the acoustic returns, generates an "omega" effect.

Of all the artifacts discussed here, "omega" effects are the most likely to mislead investigators because they often appear as geologically plausible volcanic, tectonic, or even depositional (mass-wasting) features. An "omega" on the side of a seamount as in Plate 1*c*, could possibly be mistaken for a flank or satellite construct. Irregular "omega"-type artifacts (Plate 1*f*) appearing on what are actually relatively straight scarps might be misinterpreted as changes or variations in structural trend. This could result in errors in determining the tectonic character and evolution of an area. Other "omegas" (Plate 1*e*) might be mistaken for volcanic constructional features and incorrect conclusions could be reached regarding post-tectonic or syntectonic volcanism on scarps such as fracture zone

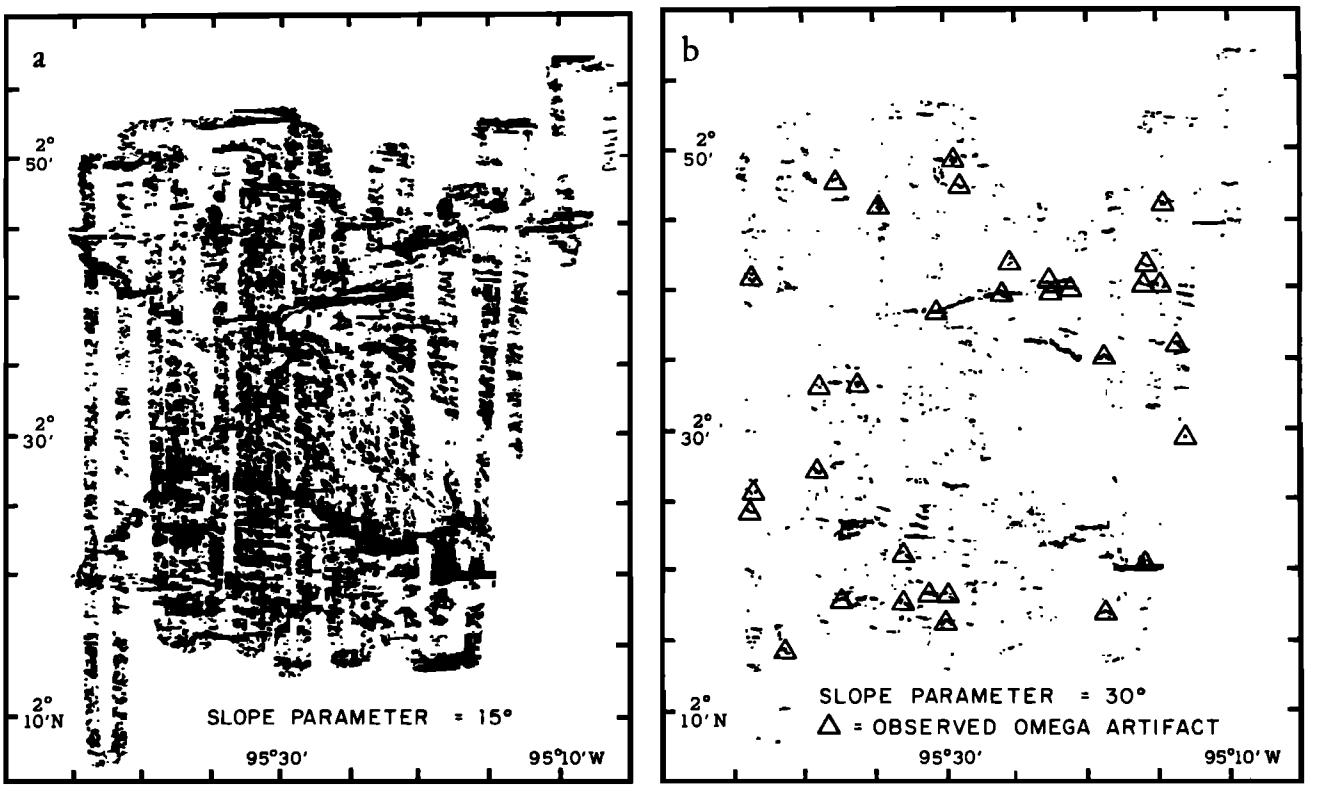

Fig. 13. Bathymetric gradient charts of Sea Beam data from Galapagos 95.5°W propagating rift survey (modified from *Hey et al.*, [this issue]). All areas where five-ping-averaged Sea Beam data exhibit slopes greater than the slope parameter (specified in the lower right of each plot in degrees from the horizontal) are darkened. (*a*) Slope parameter = 15°. Data coverage and tectonic fabric (mostly E-W, see *Hey et al.*, [this issue] for discussion) of this rugged terrain are visible in this plot. (*b*) Slope parameter = 30°. Triangles show locations of features appearing on this plot that are associated with "omega" artifacts seen in 20-m contour plots.

walls, rift valley walls, pseudofault walls, abyssal hill scarps, caldera walls, etc. In addition, some "omegas" might be mistaken for serpentinite diapirs, while others (for example, at trenches or submarine canyons) could be erroneously identified as slump blocks or other mass-wasting deposits. When dealing on scales of hundreds of meters to several kilometers, failing to recognize "omegas" as artifacts could lead to errors in geologic understanding because they might suggest unexpected volcanism or tectonism in supposedly inactive areas. The implications of these possible misinterpretations are very important.

Suspicious features which have the characteristic shape of "omegas" have been observed in data from every Sea Beam survey we have investigated thus far. Many geophysical surveys are run orthogonal to the tectonic fabric because important variations in magnetic, seismic, gravity, and bathymetric data often are found in cross-strike profiles. Unfortunately, because "omegas" are found on downdip tracks, this type of survey pattern increases the probability of occurrence of these artifacts. In an effort to quantify this probability, we have analyzed data from such a survey (Figure 13). Figure 13 shows Sea Beam data from the propagating rift at 95.5°W on the Cocos-Nazca spreading center [*Hey et al.*, this issue]. In Figure 13, all areas where the gradient of the bathymetry, as detected by Sea Beam, exceeds a specified slope are darkened. Figure 13*a* is included mainly to show the data density and the overall tectonic structure. The "omega" effect was discovered while analyzing this dense data set with several overlapping swaths and the "omegas" shown in Plate 1 are examples of artifacts that Hey and coworkers removed from their data. In eight cases for which we initially suspected the "omega" bathymetry to be false and then studied the acoustic data, our suspicions were confirmed. By checking the raw Sea Beam data, we have identified eight others. We then estimated the probability of encountering "omegas" on downdip tracks over fairly steep slopes. We have visually examined the computer-generated Sea Beam 20-m contour plots and identified all the "omegas" which we feel confident are artifacts (many questionable examples were also found but were not included in the exercise). Triangles in Figure 13*b* mark the locations where features on this plot are associated with "omegas" seen in the contour plots. Knowing the direction of ship's travel, we were able to distinguish on Figure 13 those downdip slope crossings which have "omega" artifacts and those which do not. For approximately 50% of all occurrences where the ship steamed downdip across slopes which Sea Beam detected as being greater than 30°, "omega" artifacts are present. Though we realize that these estimates are rough, the salient point is clear: "omega" artifacts can be very common in conventional surveys which run perpendicular to the tectonic fabric. As mentioned above, the frequency of occurrence

of these artifacts may vary with each Sea Beam system depending on the side lobe level of its transmit beam pattern, as well as with ship's speed.

Our detailed analysis of these artifacts has concentrated on the SIO Sea Beam system because of the availability of its acoustic data. But we have observed "omega"-like features in bathymetric data collected with systems aboard the R/V's *Conrad* (Lamont-Doherty Geological Observatory), *Surveyor* (National Oceanographic and Atmospheric Administration), and *Jean Charcot* (IFREMER). Sea Beam investigators who see suspicious features with characteristics similar to the "omegas" shown here would be prudent to survey the sites with crossing Sea Beam swaths for confirmation before attributing them great significance or planning higher-resolution studies. If such features are not recognized as potentially important until after the survey, the raw Sea Beam data should be checked, looking for unrealistic depth changes from one ping to the next and for missing data points which indicate that the system lost tracking of the bottom during that time.

Although we have only analyzed data from the Sea Beam system, we believe similar multibeam echo sounders might output the same artifacts. The U.S. Navy SASS system has been in operation since 1965, and some of its data has been declassified for use on the Mid-Atlantic Ridge Rift Valley [*Phillips and Fleming*, 1978; *Ballard and van Andel*, 1977] and on the Galapagos Rift at 86°W [*van Andel and Ballard*, 1979; *Crane and Ballard*, 1980]. Comparison of SASS bathymetry with Deep-Tow bathymetry [*Crane*, 1978; *van Andel and Ballard*, 1979] seems to indicate that "omega"-like artifacts exist in SASS data. Data gaps and onsets of "omegas" similar to those of Plate 1*b* are also apparent in the work by *Phillips and Fleming* [1978, Figure 3D].

4. POSSIBLE CORRECTIONS

Depths and cross-track horizontal distances cannot be recomputed as a postprocessing operation unless the acoustic data are digitized and recorded on tape as was done for our data. Therefore investigators discovering fictitious bathymetry in their data have no alternative but to disregard the portion of data affected. Also, these artifacts occur too infrequently to warrant recording of the acoustic data on a routine basis. Rather than relying on data reprocessing, it seems more sensible to deal with the problems at their source. In the following, we suggest a number of solutions to the problems discussed in the previous section.

4.1. *Possible Corrections for Side Lobe Interference*

When a "tunnel" effect develops during a survey, it is common practice to switch the EP from mode 3 to mode 2 [*Smith*, 1983]. As a result, the automatic tracking gates open to their maximum (upper and lower limits of the CRT display) according to parameters set by the Sea Beam operator. A subsequent return to mode 3 resumes automatic tracking. This method has proven effective in dealing with the "tunnel" effect which is essentially side lobe response related. However, it relies on the vigilance of an operator, and it will not correct the effect pointed out by *Renard and Allenou* [1979]. In general the current side lobe response suppression technique suffers from the saturation in the EP receivers. A simple modification of the detection amplifiers may solve the saturation problem, but use of logarithmic detection amplifiers to increase the EP receivers' dynamic range seems desirable [*de Moustier*, 1985*a*]. At present, there is no way to control the performance of the amplitude shading in the receiver array. As an example, we changed the shading coefficient by 30% on four array elements in the computed beam pattern of Figure 2*b*. It brought the side lobe level from 30 to 23 dB below the main lobe. This may not appear to be significant since the side lobe threshold computation is based on a value of 12 dB below a peak amplitude, which is approximately the side lobe level of an unshaded array (Figure 2*b*). However, we believe that ensuring optimum performance of the array amplitude shading can only benefit any subsequent side lobe response rejection scheme.

As the EP works on the rectified envelope of the return signals, it has no way of differentiating between side lobe response and actual bottom return when the two overlap. To tell them apart requires phase information which is not available to the EP in the current mode of operation. One way to deal with this problem would be to heterodyne (multiply by an external oscillator frequency and filter in the desired frequency band [*Clay and Medwin*, 1977]) each of the 16 preformed beam channels to obtain 16 channels of complex data (32 channels of real data). These could be digitized and processed as currently done in the EP. It would then be possible to apply advanced adaptive filtering techniques [*McCool and Widrow*, 1977] to effectively cancel side lobe response as well as noise bursts while retaining the real bottom return signal. Of course, such a scheme might be hampered by the processing time required, and it needs to be tested.

4.2. *Possible Corrections for Interference From External Sound Sources*

Whenever the 3.5-kHz echo sounder is run in conjunction with Sea Beam aboard the R/V *Thomas Washington*, the analog graphic recorder is used to display both the Sea Beam center beam profile and the 3.5-kHz echo sounder outgoing pulse. Interference occurs when the corresponding signal traces intersect. To prevent this, it is necessary to phase delay the 3.5-kHz outgoing pulse enough to keep the two traces separated [*Smith*, 1983]. This method is not entirely reliable since it requires an operator. A more reliable method consists of using a simple electronic circuit which gates out 3.5-kHz transmission whenever a Sea Beam reception cycle is in progress. Such a device reportedly works well on the R/V *Conrad* [*Tyce*, 1984]. Unfortunately, this device will not prevent interference from 12-kHz transponders, pingers, or seismic sound sources. The latter usually cannot be phase delayed for mechanical reasons (constant pulse energy requirement) as well as data postprocessing reasons (constant firing rate requirement). A solution which takes into account the transmission rate requirements of all possible underwater sound sources available aboard a ship can be implemented on the

shipboard computer. With a knowledge of the water depth, the computer would decide the best firing sequence necessary to keep the sound sources from interfering with each other (J. L. Abbott, SIO, personal communication, 1984).

4.3. *Possible Corrections for "Omega" Effects and Data Gaps*

"Omegas" and data gaps are dealt with in the same way the "tunnel" effect is, by switching the EP from mode 3 to 2 and back again. However, there is no way to detect an "omega" effect in real time since the cross-track bottom profiles on the CRT appear to be within the gates, and by the time evidence of it is seen on the swath plot it is usually too late to correct anything. The automatic tracking gate software was modified by the manufacturer in October 1984 on the system installed aboard the German R/V *Polarstern* (W. Capell, General Instrument Corporation, personnel communication, 1984). The changes consisted of increasing the minimum allowable width for each gate and enabling a faster rate of change of the gates from ping to ping. Sea Beam systems installed since October 1984 benefit from this modification which has proven effective in substantially reducing the problems of data gaps and "omega" effects. However, the widening of the bottom-tracking gates tends to decrease the depth determination accuracy on the outer beams because the remaining side lobe response is no longer gated out on those beams.

Because of the side effects of the EP receivers' calibration, mentioned in section 3.3, we recommend that an additional change be made to allow the gates to widen during a calibration cycle. This way a coincidental increase of bottom slope will easily be accommodated by the EP upon return to a normal reception cycle. Also, it would be useful to have the half hour calibration, which is triggered upon interrupt from the Sea Beam computer clock, wait for the completion of the transmission cycle in progress, and avoid situations such as that of Figure 12. Data would then be lost for only one transmission cycle, and the updating of the tracking gates would be more reliable.

Finally, as for the receiver array, some measure of the performance of the projector array amplitude shading seems necessary. At present, the system tests the performance of the power amplifiers on an all or nothing (blown fuse) basis. *Tyce* [1984] reported deviations from the manufacturer's specifications by as much as 40% on the outputs of four projector elements for the system installed aboard the R/V *Conrad*. For comparison a change of 40% in the shading coefficients of four elements in the computed beam pattern (Figure 2*a*) moved the side lobe level from 30 to 22 dB below the main lobe. Such levels will definitely enhance the signal to noise ratio of early specular returns discussed in section 3.3. (Figure 10), increasing the probability of "omegas."

5. CONCLUSIONS

In conclusion, we would like to stress the importance of a clear understanding of the capabilities and limitations of the Sea Beam system when analyzing its output. We fully recognize the value of Sea Beam bathymetry in conducting a survey and in describing abyssal morphology. This paper attempts to make the scientific community aware of a number of bathymetric artifacts observed in Sea Beam data which, if unrecognized, might lead to geological misinterpretations. We have shown that artifacts due to external sound sources (e.g., subbottom profilers) or internal side lobe interference can usually be clearly identified as resulting from spurious data. In most of these cases, corrective action can be taken in real time while surveying. We also discussed a more insidious artifact (the "omega" effect) which is virtually impossible to detect in real time for lack of warning. In addition, such artifacts commonly found when steaming downdip over slopes greater than 30° may appear as geologically plausible volcanic, tectonic or sedimentary features. When navigation is based on seafloor morphology, failure to recognize bathymetric artifacts may lead to positioning errors.

In order to explain the causes of these artifacts, we have analyzed Sea Beam's echo detection and processing techniques. Errors have been found to relate to the methods of side lobe rejection, automatic bottom-tracking, and automatic receiver gain calibration. These errors result in incorrect depth determinations which cause the artifacts observed. Because Sea Beam only retains depths and cross-track horizontal distances from the received acoustic signals, investigators have no alternative but to disregard the bathymetric artifacts they identify. A number of corrections are proposed to prevent such data disposal: improved side lobe control in the transmit/receive acoustic geometry, extension of the EP receivers' dynamic range, side lobe and noise burst rejection through advanced adaptive filtering techniques, improved bottom-tracking gate operation, delayed receivers' gain calibration to allow for completion of the reception cycle in progress, and computer-coordinated signal transmission for all active sound sources during a survey.

Recently, presentation formats for Sea Beam data have extended beyond contour maps to include gray-tone and color shaded relief maps [*Edwards* et al., 1984], and bathymetric gradient charts [*Hey et al.*, this issue]. These formats are very valuable in interpreting the data; however, "omegas" and other bathymetric artifacts will persist because the errors are in the raw Sea Beam data, not in the contouring algorithm employed.

APPENDIX A: SEA BEAM ACOUSTIC GEOMETRY

In the following, the beam widths are calculated at the half power point of the beam patterns. The transmitted beam pattern spans 54° athwartships by 2 2/3° in the fore-aft direction. It is pitch stabilized to ensure vertical projection by phasing the outputs of the 20 power amplifiers relative to a pitch angle supplied by the vertical reference gyroscope (Figure 1) within the limits of ±10° of pitch. As shown in the computed beam pattern (Figure 2*a*), the projector array is designed for side lobe attenuation 30 dB down from the main lobe and grating lobes appear at 55° on the fore-aft axis. The side lobe level is controlled by amplitude shading the output of the 20

power amplifiers (Figure 1) using the Dolph-Chebyshev amplitude shading method for acoustic arrays [*Dolph*, 1946; *Riblet and Dolph*, 1947]. Since the array is contained in a housing, the actual side lobe level is 25-26 dB down from the main lobe [*Dolph* 1946; *Renard and Allenou* 1979]. Proper control of the side lobes on the transmitted beam in the fore-aft direction is crucial for adequate performance of the system when the ship's track runs down-dip (across a slope in the downhill direction). In this geometry, weakly attenuated side lobes ensonify the slope at near-normal incidence in the fore-aft direction. The corresponding bottom returns are received earlier than those due to vertical projection in the main lobe, and they disrupt the echo-processing and bottom-tracking functions.

The design of the receiving array yields a beam pattern which is 2 2/3° athwartships by 20° in the fore-aft direction (Figure 2*b*). The 20° beam width in the fore-aft direction is meant to accommodate pitch angles of ±10°, as no pitch stabilization is performed on the receiving beams. Sea Beam generates 16 preformed beams fixed with respect to the ship's vertical by electronically steering such 2 2/3° beams at intervals of 2 2/3° athwartships from 20° incidence on port to 20° on starboard. Dolph-Chebyshev amplitude shading of the output of the 40 preamplifiers (Figure 1) attenuates the side lobes 30 dB below the main lobe (Figure 2*b*). For the same reasons given for the projector array, the actual side lobe level may be somewhat higher. *Renard and Allenou* [1979] measured a value of 28 dB on two preformed beams. The acoustic data we have recorded indicate a mean side lobe level of 25 dB below the main lobe on 10 preformed beams for the SIO system [*de Moustier*, 1985*b*]. Proper side lobe level control is important for the receiving array because each of the preformed beams has side lobes oriented in the direction of the main lobe of all the other beams. A strong return coming into the main lobe of a particular beam will therefore be received by all the side lobes pointing in the same direction.

APPENDIX B: SEA BEAM ECHO PROCESSING

Information concerning Sea Beam's echo processing is contained in the Sea Beam software technical manual [*General Instrument Corporation*, 1981]. In the following, we give, with the manufacturer's permission, an overview of the main features of the echo-processing software. We emphasize the features important to understand the causes of the bathymetric artifacts discussed in this paper.

During each transmission cycle, 16 bottom returns (e.g., Figure 3) are digitized by Sea Beam's analog-to-digital converter at a frequency of 300 Hz for each beam. For each conversion cycle the Sea Beam computer performs the following operations: receiver gain correction, refraction correction, roll compensation, detection threshold level determination, and signal detection for each of the roll-compensated beams.

The receiver gain correction consists of multiplying the digitized signal voltage for each beam by an amplitude multiplication factor to compensate for differences among receivers. Because the roll compensation involves interpolation between beams, it is important that all 16 signals have a common gain at any one time. The gains of the individual receivers are automatically calibrated by the EP every half hour by inputting a common voltage through the beam line drivers (Figure 1) and digitizing the output of the receivers.

The refraction correction uses values of a sound velocity versus water depth profile, entered at the beginning of a survey by the Sea Beam operator, and Snell's law to calculate the reception angle Θ for each beam with respect to the ship's vertical. The sound velocity profile is measured with an expendable bathythermograph cast for the first few hundred meters and extended to the maximum bottom depth in the survey area using values from Carter's tables of sound velocity in the ocean [*Carter*, 1980].

The roll compensation uses the ship's instantaneous roll angle β given by the vertical reference gyroscope to reference the reception angle Θ to the true vertical: $\Phi = \Theta + \beta$. A set of stabilized beams angles Ψ spaced 2 2/3° apart are then created. The amplitudes of the stabilized beams are linearly interpolated between those of the two adjacent preformed beams with reception angle Φ_i and Φ_{i+1}. This yields 15 stabilized beams each 2 2/3° wide, fixed in a vertical plane athwartships with one beam aligned with the true vertical. As provision has been made for ±20° of ship's roll, there are 31 possible stabilized beam positions between ±40°. Occasionally, one of the preformed beam angles Φ will lie on the true vertical ($\Psi = 0$), and there may be 16 stablized beams.

A set of bottom-tracking gates determines the detection time window during which a bottom echo is expected based on previous sounding history. The tracking gate is an essential feature of the EP because it conditions proper echo signal detection and therefore reliable depth determination. Each beam has its own tracking gate. It is centered on the average depth for that beam using depth history over the last five transmission cycles (pings) weighted decreasingly into the past. The gate width is determined by the observed ping-to-ping depth fluctuations with allowance for variations in signal duration due to beam angle, bottom slope, and beam width. As a result, the gates are narrower for the near-vertical beams than for the outer beams. A constant value (20 m) is added to the width of each gate as a safety margin to ensure that the echo signal does not fall outside the gate. Bottom echoes falling outside the tracking gates are not taken into account by the EP which usually will not compute a depth and a cross-track distance for the corresponding beams for lack of signal to noise ratio. This situation creates a data gap. Since only 15 (occasionally 16) of the possible 31 stabilized beams bear data, gate settings for null or unused beams are interpolated or extrapolated from those of adjacent beams. Finally, the gate settings are smoothed across all 31 possible beams. The analog-to-digital conversion starts at the onset of the gate with the shallowest setting (earliest time). The conversion stops when the deepest gate has been reached.

The detection threshold level determination is a very critical operation in the echo processing. It is adjusted every conversion cycle and is therefore a dynamic process taking several parameters into consideration: (1) the manual threshold level input by the Sea Beam operator, (2) the background noise level of the receivers, (3) the

receivers' side lobe response, and (4) potential noise bursts interfering with the bottom echo detection. In general, the threshold level is computed to ride above the noise and above the side lobe response. For reference, the noise level measured on data similar to that of Figure 3 is usually around 20 mV. The side lobe threshold is computed as one-fourth the amplitude (12 dB down) of the highest of the 16 signals at any one time (Figure 3). A noise burst appears as a synchronous ridge similar to the side lobe ridge of Figure 3, but the amplitudes of the individual peaks are more or less constant on all beams (e.g., Figure 7). By comparing the maximum amplitude with the median amplitude across all beams at any one time, the software is able to recognize a noise burst. When a noise burst is detected, and when the corresponding threshold level is higher than both the noise and the side lobe thresholds, the 16 amplitudes are rejected. Otherwise, the higher of the noise or the side lobe thresholds will be used as the detection threshold. With this method, however, canceling side lobe response or noise bursts when they overlap with a bottom return results in cancellation of the corresponding part of the bottom return. Also, because of saturation in the EP receivers' amplifiers, side lobe rejection is only partially achieved in cases when the specular return is clipped. This results in both echo detection and depth computation errors. Finally, for each conversion cycle, a signal sample is detected if it is above the detection threshold and within the bottom-tracking gates.

Once the analog-to-digital conversion sequence has been completed on all beams, the next set of echo-processing operations is done once per transmission cycle. The signal level of each detected beam is integrated over the duration of the detected return (within the gates and above the threshold). If the resulting energy in the return is below a prescribed minimum, the beam is deemed invalid due to poor signal to noise ratio [*Farr*, 1980]. For a valid beam, a slant range is calculated by computing the center of mass of all the detected signal samples for that beam, and by multiplying the corresponding arrival time by 750 m/s. Depth and cross-track horizontal distances are then calculated as described in section 2.

Acknowledgments. The work reported here would not have been possible without the cooperative efforts of the captain and crew of the R/V *Thomas Washington*. We wish to thank W. Capell from General Instrument Corporation for his patience in answering our numerous questions; R. N. Hey, P. F. Lonsdale, J. L. Abbott, T. H. Shipley, and P. C. Henkart for helpful comments and data samples; R. C. Tyce for initiating the Sea Beam acoustic backscattering experiment at MPL; and F. V. Pavlicek for his support during the development of the Sea Beam acoustic data acquisition system. We are indebted to R. N. Hey, K. Crane, J. A. Hildebrand, and S. P. Miller for their valuable suggestions and critical review of the manuscript. We are also grateful to J. Barron and E. Ford for typing and editing and J. Griffith for the art work. For their support, we thank the Office of Naval Research (contract N00014-79-C-0472) and the National Science Foundation (grant OCE-8109927).

References

Ballard, R. D. and T. H. van Andel, Morphology and tectonics of the inner rift valley at lat. 36°50N on the Mid-Atlantic Ridge, *88, 507-530, 1977.*

Ballard, R. D. and J. Francheteau, Geologic processes of the mid-ocean ridge and their relation to sulfide deposition, in *Hydrothermal Processes at Seafloor Spreading Centers,* pp. 17-26, Plenum, New York, 1983.

Carter, D. J. T., *Echo-Sounding Correction Tables,* Hydrographic Department, Ministry of Defence, Somerset, U.K., 1980.

Clay, C. S. and H. Medwin, *Acoustical Oceanography: Principles and Applications,* p. 128, John Wiley, New York, 1977.

Crane, K., Structure and tectonics of the Galapagos Inner Rift, 86°10'W, *J. Geol., 86,* 715-730, 1978.

Crane, K. and R. D. Ballard, The Galapagos Rift at 86°W', Morphological waveforms, 4, Structure and morphology of hydrothermal fields, *J. Geophys. Res., 85,* 1443-1454, 1980.

Crane, K., F. Aikman, R. Embley, S. Hammond, A. Malahoff, and J. Lupton, The distribution of geothermal fields on the Juan de Fuca Ridge, *J. Geophys. Res., 90,* 727-744, 1985.

de Moustier, C., Inference of manganese nodule coverage from Sea Beam acoustic backscattering data, *Geophysics, 50,* 989-1001, 1985*a*.

de Moustier, C., Beyond Bathymetry, mapping acoustic backscattering from the deep seafloor with Sea Beam, *J. Acoust. Soc. Amer., (in press),* 1985*b*.

Detrick, R. S., P. J. Fox, K. Kastens, W. B. F. Ryan, L. Mayer, and J. Karson Mid-Atlantic Ridge Rift Valley, A Sea Beam survey of the Kane Fracture Zone and the adjacent, *EOS, Trans. AGU, 65,* 1006, 1984.

Dolph, C. L., A current distribution of broadside arrays which optimizes the relationship between beam width and side-lobe level, *Proc. Inst. Radio Eng., 34,* 335-348, 1946.

Edwards, M. H., R. E. Arvidson, and E. A. Guiness, Digital image processing of Sea Beam bathymetric data for structural studies of seamounts near the East Pacific Rise, *J. Geophys. Res., 89,* 11108-11116, 1984.

Farr, H. K., Multibeam bathymetric sonar: Sea Beam and Hydrochart, *Mar. Geol., 4,* 77-93, 1980.

Fornari, D. J., W. B. F. Ryan, and P. J. Fox, The evolution of craters and calderas on young seamounts: Insights from Sea MARC I and Sea Beam sonar surveys of a small seamount group near the axis of the East Pacific Rise at ~10°N, *J. Geophys. Res., 89,* 11069-11084, 1984.

Francheteau, J. and R. D. Ballard, The East Pacific Rise near 21°N, 13°N and 20°S; inferences for along strike variability of axial processes, *Earth Planet. Sci. Lett., 64,* 93-116, 1983.

Gallo, D. J., P. J. Fox, and J. A. Madsen, The morphotectonic signature of fast-slipping ridge-transform-ridge systems: A synthesis of Sea Beam bathymetry, *EOS Trans. AGU, 65,* 1103, 1984.

General Instrument Corporation, *Sea Beam bathymetric survey system, Technical Manual, Vol. 2,* Westwood, Mass., 1981.

Glenn, M. F., Introducing an operational multi-beam array sonar, *Int. Hydrogr. Rev., 47(1),* 35-39, 1970.

Hey, R. N., M. C. Kleinrock, S. P. Miller, T. M. Atwater, and R. C. Searle, Sea Beam/Deep-Tow investigation of an active oceanic propagating rift system, *J. Geophys. Res.,* (this issue).

Hey, R. N., D. F. Naar, M. C. Kleinrock, W. J. Phipps Morgan, E. Morales, and J. G. Schilling, Microplate tectonics along a superfast seafloor spreading system near Easter Island, *Nature, 317,* 320-325, 1985.

Kleinrock, M. C., R. N. Hey, and C. de Moustier, The "Omega" deception in Sea Beam data, *EOS Trans. Am. Geophys. Union, 65,* 1103, 1984.

Lewis, S. D., J. W. Ladd, T. R. Bruns, D. E. Hayes, and R. Von Huene, Growth patterns of submarine canyons and slope basins, Eastern Aleutian Trench, Alaska, *EOS Trans. Am. Geophys. Union, 65,* 1104, 1984.

Lonsdale, P. F., Overlapping rift zones at the 5.5°S offset of the East Pacific Rise, *J. Geophys. Res., 88,* 9393-9406, 1983.

Macdonald, K. C. and P. J. Fox, Overlapping spreading centers: A new kind of accretion geometry on the East Pacific Rise, *Nature, 301,* 55-58, 1983.

Macdonald, K. C., J. C. Sempere, and P. J. Fox, East Pacific Rise from Siqueiros to Orozco fracture zones: Along-strike continuity of axial neo-volcanic zone and structure and evolution of overlapping spreading centers, *J. Geophys. Res., 89,* 6049-6069, 1984.

Mammerickx, J., Morphology of propagating spreading centers:

New and old, *J. Geophys. Res., 89,* 1817-1828, 1984.
McCool, J. M. and B. Widrow, Principles and applications of adaptive filters: A tutorial review, *NUC TP 530,* Nav. Ocean Syst. Cent., San Diego, CA., 1977.
Naar, D. F. and R. N. Hey, Fast rift propagation along the East Pacific Rise near Easter Island, J. Geophys. Res., (this issue).
Patterson, R. B., Relationships between acoustic backscatter and geological characteristics of the deep ocean floor, *J. Acoust. Soc. Am., 46,* 756-761, 1969.
Phillips, J. D. and A. S. Fleming, Multibeam sonar study of the MAR Rift Valley 36-37°N, Map Series MC-19, *Geol. Soc. of Amer.,* Boulder, Colo., 1978.
Renard, V. and J. P. Allenou, SEA BEAM multi-beam echosounding in "Jean Charcot". Description, evaluation and first results, *Int. Hydrog. Rev., 56(1),* 35-67, 1979.
Riblet, H. L. and C. L. Dolph, Discussion on a current distribution of broadside arrays which optimizes the relationship between beam width and side-lobe level, *Proc. Inst. Radio Eng., 35,* 489-492, 1947.
Shipley, T. H. and G. F. Moore, Sediment accretion and subduction in the Middle America Trench, *OJI International Seminar on the formation of ocean margins,* Ocean Research Institute, University of Tokyo, Tokyo, Japan, 1985.
Smith, S. M., Sea Beam Operator Manual, SIO Reference 83-7, Scripps Institution of Oceanography, La Jolla, Calif., 1983.
Spiess, F. N. and P. F. Lonsdale, Deep-Tow rise crest exploration techniques, *Mar. Technol. J., 16,* 67-75, 1982.
Spiess, F. N., R. Hessler, G. Wilson, M. Weydert, and P. Rude, Echo I cruise report, SIO Ref. 84-3, Scripps Institution of Oceanography, La Jolla, Calif., 1984.
Tyce, R. C., Sea floor mapping aboard R/V *CONRAD* - The first year of Sea Beam, *EOS Trans. AGU, 65,* 1103, 1984.
Urick, R. J., *Principles of Underwater Sound, 3rd edition,* McGraw-Hill, New York, 1983.
van Andel, T. H. and R. D. Ballard, The Galapagos Rift at 86°W, 2, Volcanism structure and evolution of the Rift valley, *J. Geophys. Res., 84,* 5390-5406, 1979.

C. de Moustier, Marine Physical Laboratory, A-005, Scripps Institution of Oceanography, University of California, San Diego, La Jolla, CA 92093.

M. C. Kleinrock, Geological Research Division, A-020, Scripps Institution of Oceanography, University of California, San Diego, La Jolla, CA 92093

(Received January 4, 1985;
revised August 2, 1985;
accepted August 7, 1985.)

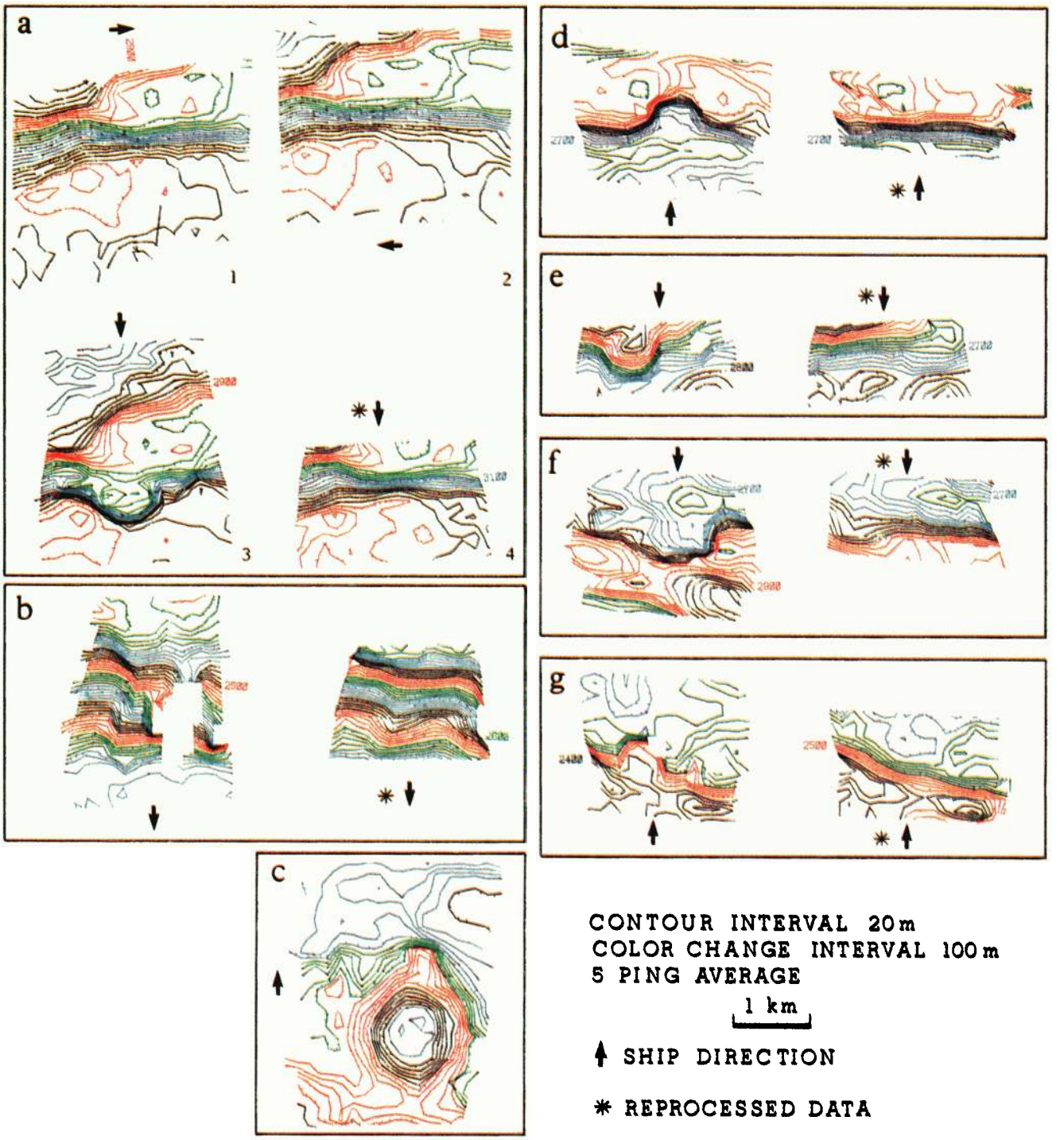

Plate 1. [*de Moustier and Kleinrock*] "Omegas" and gaps. Tick marks point downhill. Contoured sections not starred are original Sea Beam data. Contoured sections marked with a star are the result of reprocessing the acoustic data recorded digitally with the MPL system. Our simplified echo-processing technique does not include ray-bending corrections, and arrival times are determined by the first arrival above a preset threshold. The threshold level is selected after visual inspection of the roll-compensated acoustic data. Recomputed depths and cross-track distances are therefore in uncorrected meters referenced to a sound velocity of 1500 m/s. Although crude, this processing method suffices to prove the fictitious character of Sea Beam's contoured bathymetry shown in Plates 1*a*, (section 3), 1*b*, 1*d*, 1*e*, 1*f* and 1*g*. We do not show a recomputed version of Plate 1*c* because the corresponding acoustic data was only recorded every five pings. This was enough to confirm the "omega" effect, but contour resolution was seriously degraded by the five ping decimation.